Coherent Combining of Phase-Steerable High Power Microwaves Generated by Two X-Band Triaxial Klystron Amplifiers with Pulsed Magnetic Fields

Jinchuan Ju,[*,†] Xingjun Ge,[†] Wei Zhang,[†] Fangchao Dang, Yunxiao Zhou, Fuxiang Yang, Chengwei Yuan, Xinbing Cheng, Qiang Zhang,[‡] and Juntao He[§]

College of Advanced Interdisciplinary Studies, National University of Defense Technology, Changsha 410073, China

(Received 1 November 2022; revised 18 January 2023; accepted 31 January 2023; published 24 February 2023)

We report the first experimental demonstration of coherent combining of phase-steerable high power microwaves (HPMs) generated by X-band relativistic triaxial klystron amplifier modules under the guidance of pulsed magnetic fields. Electronically agile manipulation of the HPM phase is achieved with a mean discrepancy of 4° at the gain level of 110 dB, and the coherent combining efficiency has reached as high as 98.4%, leading to combined radiations with equivalent peak power of 4.3 GW and average pulse duration of 112 ns. The underlying phase-steering mechanism during the nonlinear beam-wave interaction process is furthermore explored by particle-in-cell simulation and theoretical analysis. This Letter paves the way for high power phase array in large scale and may stimulate new interest in research of phase-steerable high power masers.

DOI: 10.1103/PhysRevLett.130.085002

High power microwaves (HPMs), particularly referring to the electromagnetic radiations with peak power over 100 MW and frequency ranging from 1 to 300 GHz [1], have numerous applications in fields such as particle acceleration [2], wakefield generation [3,4], nuclear fusion [5–7], and space propulsion [8]. Nevertheless, power capacity of an individual HPM source is intrinsically restricted by the issues of breakdown, which roughly obeys the scaling law $P \propto f^{-2}$ [9,10], implying a low power P at a high frequency f. A promising approach to overcome the power limit is combining N sources coherently to achieve enhanced power density in far field with increase gain of N^2 [1]. Because of the difficulties in phase control over the radiations emitted by intense relativistic quasifree electron beams [11], only a few attempts of HPM coherent combining have been made [12–16]. A popular scheme was to combine HPM oscillators driven by a common accelerator, which relies on either mutual coupling beyond Adler's threshold [17] in steady state [12] or shock leading edge of transient superradiance [13–15] to correlate the emission phases. Nevertheless, this combining scheme can hardly be generalized to large scale owing to practical and physical problems such as dispersion [18]. The next-generation HPM coherent combining scheme would be based on the master oscillator power amplifier (MOPA) method energized by independent accelerators [1], which is similar but more challenging than conventional phase array. Apart from synchronization in time, the MOPA approach requires agile phase steering, beyond phase locking, of each HPM source to achieve constructive interference, as well as beam scanning, and a pulsed guiding magnetic field to reduce energy consumption in large arrays. The challenge in agile phase steering is sophisticated manipulation of the emission process of intense electron beams from the onset stage of steady state. The difficulties that lie behind guidance with pulsed magnetic field are the complex influences of eddy current, skin effect, and field penetration time through mixed materials in field magnitude and profile [1,19–21].

In this Letter, we present for the first time coherent combining of phase-steerable X-band HPMs generated by two high power amplifier modules under the guidance of pulsed magnetic fields. Electronically agile phase steering is demonstrated on a shot-to-shot basis at the master power level down to −110 dB when the pulsed magnetic field is 0.4 T. The achieved coherent combining efficiency is 98.4%, yielding an equivalent peak power of 4.3 GW in far field with pulse duration of about 112 ns. Such high power and long pulse X-band radiations have not been reached by the state-of-the-art single HPM source [22], showing promising prospects of coherent combining with the MOPA scheme. The results of particle-in-cell simulation and theoretical analysis agree well with the experimental observations. The presented research is essential for developing advanced high power phase arrays and would inspire investigations into new functionalities relying on agile manipulations of HPM phases.

The phase-steerable HPMs are generated by a relativistic triaxial klystron amplifier (TKA) [23–27] operating in X-band at 10 GHz as shown in Fig. 1(a). The TKA is surrounded by a solenoid that generates pulsed magnetic fields for beam guidance. The input cavity is a reentrant structure with cold-cavity quality factor $Q_c \simeq 180$ at the resonant frequency 10.002 GHz. The cascaded bunching1 and bunching2 cavities operate in TM_{011} and TM_{012} modes

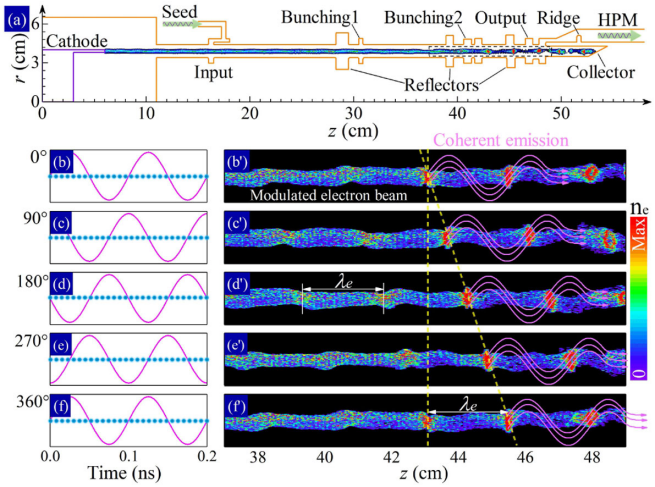

FIG. 1. (a) Schematic of the phase-steerable TKA, in which the contour plot indicates the modulated electron beam when HPM generation becomes saturated. (b)–(f) The first two periods of the seed microwave with different initial phase φ_0, where the dots represent uniformly distributed electrons passing through the input cavity gap. (b′)–(f′) The corresponding modulated electron beam distributions in the enlarged area indicated by the dashed rectangle in (a).

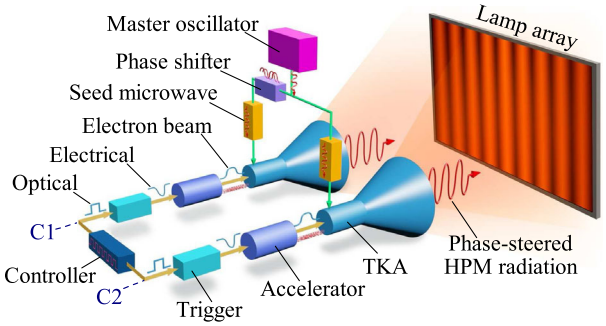

FIG. 2. Schematic diagram of the experimental arrangement, in which the lamp array can be removed to place detectors for HPM measurements. The two channels are termed as C1 and C2, respectively.

with Q_c of 400 and 580, respectively. Their associated resonant frequencies, 9.997 and 10.084 GHz, are staggered to optimize electron beam bunching. The output cavity incorporating feedback from the ridge has Q_c of 54 at the resonant frequency of 10.003 GHz (see Supplemental Material [28]). We specifically choose TM_{011} mode for the first bunching cavity in order to actively quench parasitic asymmetric modes [29], and three reflectors are placed upstream the cavities to suppress transverse-electromagnetic mode coupling [30]. The electron beam first gets gentle modulation at the input cavity gap, while the modulation is intensified dramatically after passing through the cascaded bunching cavities, leading to nearly discrete beam bunches at the output cavity where coherent emission is produced, as shown in Fig. 1. In the amplification regime, the beam modulation and emission processes are initialized and dominated by the seed microwave, which provides an opportunity to manipulate the output HPM phase. This mechanism is illustrated in Figs. 1(b)–1(f), in which the curves show the first two periods of the continuous seed microwave with its initial phase φ_0 varying at a step of 90°. Figures 1(b′)–1(f′) display the corresponding electron beam distributions at a given time in simulation (see the following part). It is clear that the electron bunches are shifted along the longitudinal axis by the seed microwaves initialized with different phases, accordingly giving rise to coherent emissions linearly steered in phase.

The experimental configuration of the phase-steerable HPM coherent combination is schematically illustrated in Fig. 2. It mainly consists of two radiation modules driven by their respective pulsed power accelerators. We first employ the C1 channel to demonstrate the phase-steering results and then turn to coherent combining of the two sources. The accelerator could provide high voltage pulses reaching 600 kV [31], and its function was triggered to achieve synchronization in nanosecond scale [32]. Driven by the high voltage pulse, a knife-edge graphite cathode produced intense annular electron beams with radius of 3.9 cm. The TKA bulk was made by stainless steel, while the input cavity was made by aluminum to reduce Ohmic loss [27]. The master oscillator generated the original microwave signal, and in the C1 branch there was a 6-bit digital phase shifter with a tuning step of about 5.6°. The seed microwave injected to the TKA was provided by a kilowatt-class klystron amplifier.

Of prime importance for guidance with pulsed magnetic fields is to achieve high field uniformity and stable electron beam transportation [19]. In previous research [21], the beam guidance was optimized by passive adjustments in experiment. Herein we have examined the complex issues of eddy current, skin effect, and field penetration time through mixed materials by simulating with computer simulation technology (CST) [33], through which temporal-spatial field distribution in the whole TKA structure has been obtained (see Supplemental Material [28]). The magnetic coils are driven by a sinusoidal current with half cycle of 18 ms in the simulation. Figure 3(a) displays temporal evolutions of the guiding magnetic fields at different positions along the electron beam path ($r = 3.9$ cm), where $z = 16$ and $z = 26$ cm are typical points corresponding to the parts of aluminum and stainless steel, respectively. One can see that the two field summits appear differently in time and both are retarded with respect to the driving current that peaks at $t = 9$ ms. Moreover, the maximal field for aluminum ($z = 16$ cm) is less than that for steel ($z = 26$ cm), so the field magnitude and profile along the beam path vary with time, as shown in Fig. 3(b). We find that the optimal time with both high field uniformity and magnitude is the cross point of the two temporal profiles as indicated in Fig. 3(a), namely,

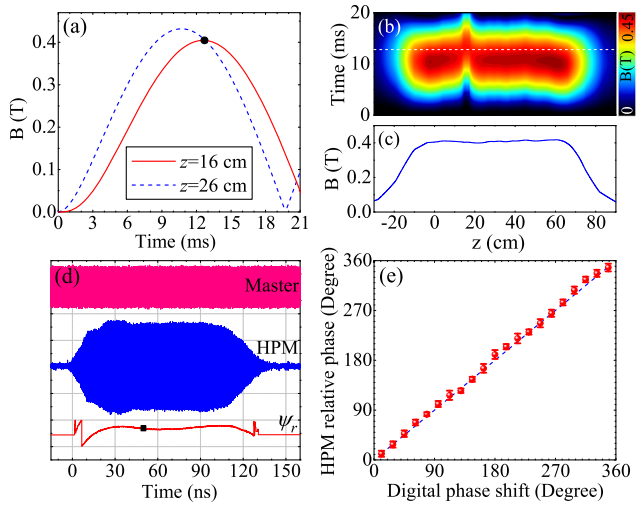

FIG. 3. Evolutions of the guiding magnetic fields (a) at different positions and (b) along the beam path. (c) The field profile at $t = 12.8$ ms indicated by the dashed line in (b). (d) Real-time waveforms of the master oscillator, HPM, and their relative phase ψ_r. The vertical scale for field is 150 mV/div and for phase is 360°/div. (e) Results of HPM phase steering, where the error bars indicate the standard deviations of 20 shots and the dashed line is the diagonal plotted as reference.

$t \simeq 12.8$ ms. In experiment, the solenoid was powered by a 2 mF capacitor charged to 1.84 kV, and the discharge current showed a peak of 425 A. As suggested by the simulation results, the electron beams were launched at $t \simeq 12.5$ ms, and the corresponding magnetic field was measured to be about 0.4 T. Nylon witness targets were placed in the TKA at different longitudinal positions, and all the electron beam imprints exhibited high azimuthal uniformity [28], implying stable beam transportation over the tube under guidance of the pulsed magnetic field.

The HPMs were radiated by a horn antenna with aperture size of 830 mm [34] and characterized in an anechoic chamber [28]. All the cables, attenuators, and crystal detectors were calibrated by a vector network analyzer. Driven by a 540 kV, 7.8 kA electron beam, the HPM power of a single source was evaluated to be approximately 1.1 GW, and the pulse duration was around 114 ns. The seed microwave power could be lowered to ~33 kW, corresponding to a gain of about 45.2 dB. Figure 3(d) displays typical real-time waveforms of the master oscillator and the HPM radiation recorded by a digital oscilloscope with 40 Gs/s sampling and $\sin(x)/x$ interpolation. The relative phase ψ_r between the two signals was calculated by postprocessing within the range of [−180°, 180°]. Figure 3(d) shows that the HPM phase is stably locked by the master oscillator, which is the preliminary condition for phase steering. We shall emphasize that no appreciable radiation was detected when the master oscillator was switched off, which indicated that the TKA indeed operated in the amplification regime. This feature distinguishes our work in terms of fundamental mechanism from the previous research based on phase-primed Cherenkov radiation [35,36].

In the phase-steering experiment, the digital phase shifter operated with a shift step of 16.9° and an error of about 1°. Without losing generality, we chose the relative phase ψ_r at $t \simeq 50$ ns as indicated by the dot in Fig. 3(d) to represent the results of HPM phase steering. The obtained relative phases were unwrapped and offset in order to make a continuous plot in the range of [0°, 360°] in Fig. 3(e). It clearly demonstrates that the HPM phases can be steered linearly by the digital phase shifter as shown in Fig. 1. The mean discrepancy of the phase steering between the experimental measurements and ideal expectations was about 4°, showing very high precision. As the master oscillator operated in 10 mW and the HPM power was 1.1 GW, we thus achieved precise phase manipulation in the gain level of about 110 dB. Each point in Fig. 3(e) corresponds to the average of 20 consecutive shots, where the error bars indicate the associated standard deviations. It is found that the mean of the standard deviations is about 6°, which corresponds to shot-to-shot fluctuation of HPM phase locking.

In the coherent combining experiment, a mode converter was placed in each channel to convert the output TM_{01} mode into TE_{11} mode with horizontal polarization. The two radiation antenna centers were spaced by 1.7 m. The receiving horn was set on the symmetry axis of the two channels about 7 m away from the source antennas. Figure 4(a) demonstrates the HPM pulse envelopes measured with a crystal detector. It is apparent that the intensity of the combined pulse was enhanced to ~4 folds that of a

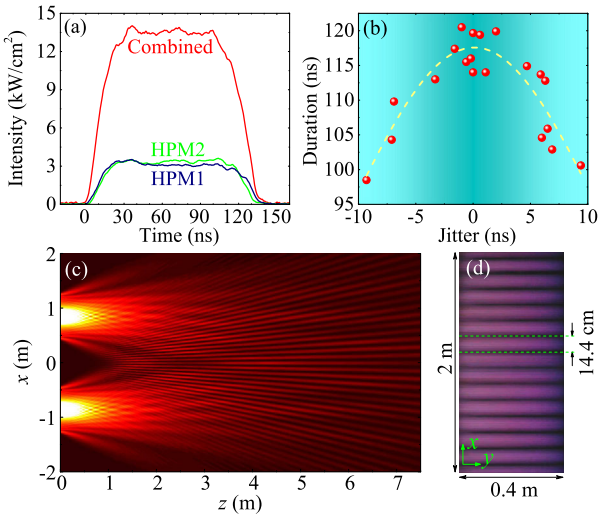

FIG. 4. (a) Typical waveforms of HPM pulses measured on the two-channel symmetry axis. (b) Dependence of the combined HPM pulse duration on the synchronization jitter of the driving high voltage pulses, and the dashed curve is Gaussian fitting. (c) Calculated field interference in the horizontal plane, and (d) displays the interference pattern measured in the transverse plane at $z \simeq 7.5$ m.

single source. The coherent combining efficiency can be calculated by

$$\eta = \frac{S_{12}}{(\sqrt{S_1} + \sqrt{S_2})^2}, \tag{1}$$

where S_1, S_2, and S_{12} are the peak intensities for the C1, C2, and combined cases, respectively. We have measured $S_1 = 3520$, $S_2 = 3537$, and $S_{12} = 13882$ W/cm^2 by averaging 20 shots for each case, which together yield a combining efficiency as high as $\eta \simeq 98.4\%$. So the equivalent peak power in far field is $1.1 \times 2^2 \times 0.984 \simeq 4.3$ GW. The C1 channel phase could be tuned agilely to achieve either constructive or destructive interference on a shot-to-shot basis, showing advanced functionality in high power beam scanning. We emphasize that synchronization between the two driving high voltage pulses does not influence the combining efficiency but the combined pulse duration. As shown in Fig. 4(b), the duration decreases when the synchronization jitter increases, and the data exhibit a Gaussian-like distribution. For the present jitter level within ± 10 ns, the average pulse duration of the 20 combined pulses is 112 ± 6.8 ns, which is nearly the same as that of a single source.

The coherent nature of the produced HPMs was examined by investigating the interference pattern. Figure 4(c) illustrates electric field distribution in the horizontal plane calculated by Fresnel-Kirchhoff's diffraction theory [37], in which the sources are extracted from the radiation aperture surface in CST simulation (see Supplemental Material [28]). We can see that the typical Young's double-slit-type interference pattern manifests during the wave propagation. Figure 4(d) displays the interference pattern of a fluorescent lamp tube (~16 mm in diameter) array with dimension of 2×0.4 m^2 illuminated by the radiation at $z \simeq 7.5$ m. The fluorescence was recorded by a video camera, and clearly visible fringes were observed, as shown in Fig. 4(d), implying high coherence of the involved HPM radiations. The interference fringe width measured in the experiment was about 14.4 cm, consisting well with the numerical result of 14.5 cm. For future applications, the combined intensity distribution can be optimized by adopting high power array antennas.

Particle-in-cell (PIC) simulation was performed with the code CHIPIC [38] to clarify the underlying physics associated with the nonlinear process of phase steering in the TKA [28]. Under the driving voltage of 550 kV, the cathode produced an electron beam of 6.9 kA. For 30 kW seed power, the output HPM power was about 1.1 GW, corresponding to a gain of 45.6 dB, which was in good agreement with the experimental results. Figure 5(a) shows that in the amplification regime the HPM phase can be steered by the seed microwave phase φ_0 from the buildup stage of the emission. When the beam-wave interaction becomes stable, the electron beam is subject to significant

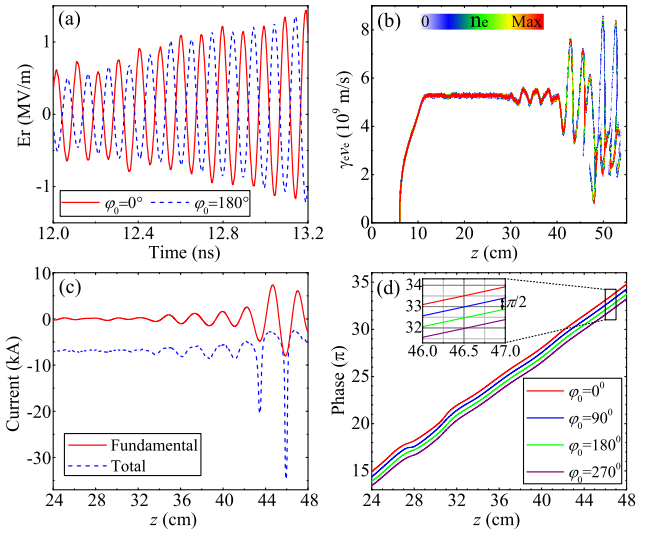

FIG. 5. PIC simulation results: (a) HPM electric field in the initial stage for φ_0 with 180° out of phase. (b) Modulated electron beam distribution in phase space and (c) the corresponding total and fundamental harmonic current profiles at $t \simeq 50$ ns. (d) The phase profiles of the fundamental harmonic currents for different φ_0, where the inset displays the details for $z \in [46, 47]$ cm.

nonlinear modulation in velocity v_e as displayed in Fig. 5(b), where it is expressed by the normalized momentum $\gamma_e v_e$ with γ_e being the relativistic factor. Figure 5(c) shows the corresponding modulated electron beam current profile $I(z)$, which has a spatial period $\lambda_e \simeq 2.5$ cm along the z axis, so $I(z)$ can be expressed as the sum of harmonics $I(z) = \sum I_n(z) = \sum \hat{I}_n(z) \cos[\phi_n(z)]$. Implementing Fourier transform on $I(z)$ and filtering in the spatial frequency domain allows us to obtain the fundamental ($n = 1$) harmonic current profile $I_1(z)$, which is also plotted in Fig. 5(c). Furthermore, by Hilbert transform, we are capable of extracting the phase component $\phi_1(z)$ contained in $I_1(z)$ [28]. It is of interest to find that, in spite of the highly nonlinear velocity modulation, the phase is delivered by the electron beam as a linear process, as shown in Fig. 5(d). The slope of the phase $\phi_1(z)$ equals the propagation constant $k_e = \omega / v_e$, with ω being the microwave angular frequency and v_e being the electron drift velocity before modulation. v_e is determined by the driving voltage and the electron beam potential in the drift tube [39]. Therefore, the relative phase fluctuation between the seed and the output microwaves can be calculated by $\Delta\psi_r = \Delta k_e \times l$, with $l \simeq 32$ cm being the distance between the input and output cavities. Considering the driving voltage instability of about 4.2 kV, $\Delta\psi_r$ has been evaluated to be 5.8°, which agrees well with the experimental measurement of approximately 6° as shown above. Furthermore, as indicated by the inset in Fig. 5(d), the $\phi_1(z)$ profiles are uniformly spaced in order by $\pi/2$, equaling the variance of the seed microwave phase φ_0, which reveals the physics of phase steering illustrated in Fig. 1.

In summary, we present the first experimental demonstration of coherent combining with two phase-steerable HPM modules driven by independent accelerators in the condition of pulsed guiding magnetic fields. The proof-of-principle coherent combination experiment achieves X-band radiations with equivalent peak power of 4.3 GW and duration of about 112 ns, which opens up new opportunities to establish large scale phase array toward generation of microwaves with unprecedented high intensity by the MOPA scheme. Furthermore, gigawatt-class HPMs with electronic agility in phase may be applied to many other fields, for example, to drive high-gradient accelerators [2] or to build coherent high power radars even with phase coding [40]. Owing to high spatial and temporal coherences of the generated HPMs, the proposed TKA functions like a seeded free-electron maser [41,42] that yields coherent radiations by stimulated emission [11]. This Letter therefore may also excite new interest in more comprehensive research in phase-steerable masers and their applications.

This work was supported by the National Natural Science Foundation of China (NSFC) with Grant No. 61771481, the Young Elite Scientists Sponsorship Program by CAST with Grant No. 20160027, and the HuXiang Young Elite Program with Grant No. 2018RS3082. We appreciate Professors Wei Liu and Tongpu Yu for their invaluable comments and suggestions.

*jujinchuan@nudt.edu.cn
†These authors contributed equally to this work.
‡119344398@qq.com
§hejuntao12@163.com

[1] J. Benford, J. A. Swegle, and E. Schamiloglu, *High Power Microwaves*, 3rd ed. (CRC Press, New York, 2016).
[2] M. A. Allen *et al.*, High-Gradient Electron Accelerator Powered by a Relativistic Klystron, Phys. Rev. Lett. **63**, 2472 (1989).
[3] G. Shafir, Ya. E. Krasik, Y. P. Bliokh, D. Levko, Y. Cao, J. G. Leopold, R. Gad, V. Bernshtam, and A. Fisher, Ionization-Induced Self-Channeling of an Ultrahigh-Power Subnanosecond Microwave Beam in a Neutral Gas, Phys. Rev. Lett. **120**, 135003 (2018).
[4] Y. Cao, Y. P. Bliokh, J. G. Leopold, A. Li, G. Leibovitch, and Ya. E. Krasik, Wake excitation by a powerful microwave pulse and its evolution in a plasma-filled waveguide, Phys. Plasmas **27**, 053103 (2020).
[5] K. R. Chu, The electron cyclotron maser, Rev. Mod. Phys. **76**, 489 (2004).
[6] M. K. A. Thumm, G. G. Denisov, K. Sakamoto, and, and M. Q. Tran, High-power gyrotrons for electron cyclotron heating and current drive, Nucl. Fusion **59**, 073001 (2019).
[7] M. Thumm, State-of-the-art of high-power gyro-devices and free electron masers, J. Infrared Millimeter Terahertz Waves **41**, 1 (2020).
[8] J. Benford, Space applications of high-power microwaves, IEEE Trans. Plasma Sci. **36**, 569 (2008).
[9] V. L. Granatstein, R. K. Parker, and C. M. Armstrong, Scanning the technology: Vacuum electronics at the dawn of the twenty-first century, Proc. IEEE **87**, 702 (1999).
[10] J. H. Booske, Plasma physics and related challenges of millimeter-wave-to-terahertz and high power microwave generation, Phys. Plasmas **15**, 055502 (2008).
[11] A. Gover, R. Ianconescu, A. Friedman, C. Emma, N. Sudar, P. Musumeci, and C. Pellegrini, Superradiant and stimulated-superradiant emission of bunched electron beams, Rev. Mod. Phys. **91**, 035003 (2019).
[12] J. Benford, H. Sze, W. Woo, R. R. Smith, and B. Harteneck, Phase Locking of Relativistic Magnetrons, Phys. Rev. Lett. **62**, 969 (1989).
[13] V. V. Rostov, A. A. Elchaninov, I. V. Romanchenko, and M. I. Yalandin, A coherent two-channel source of Cherenkov superradiance pulses, Appl. Phys. Lett. **100**, 224102 (2012).
[14] K. A. Sharypov, A. A. El'chaninov, G. A. Mesyats, M. S. Pedos, I. V. Romancheko, V. V. Rostov, S. N. Rukin, V. G. Shpak, S. A. Shunailov, M. R. Ul'masculov, and M. I. Yalandin, Coherent summation of Ka-band microwave beams produced by sub-gigawatt superradiance backward wave oscillators, Appl. Phys. Lett. **103**, 134103 (2013).
[15] N. S. Ginzburg, A. W. Cross, A. A. Golovanov, G. A. Mesyats, M. S. Pedos, A. D. R. Phelps, I. V. Romanchenko, V. V. Rostov, S. N. Rukin, K. A. Sharypov, V. G. Shpak, S. A. Shunailov, M. R. Ulmaskulov, M. I. Yalandin, and I. V. Zotova, Generation of Electromagnetic Fields of Extremely High Intensity by Coherent Summation of Cherenkov Superradiance Pulses, Phys. Rev. Lett. **115**, 114802 (2015).
[16] Z. Liu, F. Song, H. Jin, X. Jin, H. Huang, and S. Li, Coherent combination of power in space with two X-band gigawatt coaxial multi-beam relativistic klystron amplifiers, IEEE Electron Device Lett. **43**, 284 (2022).
[17] R. Adler, A study of locking phenomena in oscillators, Proc. IRE **34**, 351 (1946).
[18] N. S. Ginzburg, A. A. Golovanov, I. V. Romanchenko, V. V. Rostov, K. A. Sharypov, S. A. Shunailov, M. R. Ulmaskulov, M. I. Yalandin, and I. V. Zotova, Phase-imposed regime of relativistic backward-wave oscillators, J. Appl. Phys. **124**, 123303 (2018).
[19] M. Friedman, V. Serlin, Y. Y. Lau, and J. Krall, Relativistic klystron amplifier I—high power operation, Proc. SPIE Int. Soc. Opt. Eng. **1407**, 2 (1991).
[20] M. Yu. Glyavin, A. G. Luchinin, and G. Yu. Golubiatnikov, Generation of 1.5-kW, 1-THz Coherent Radiation from a Gyrotron with a Pulsed Magnetic Field, Phys. Rev. Lett. **100**, 015101 (2008).
[21] N. S. Ginzburg, A. M. Malkin, A. S. Sergeev, I. V. Zheleznov, I. V. Zotova, V. Yu. Zaslavsky, G. Sh. Boltachev, K. A. Sharypov, S. A. Shunailov, M. R. Ul'masculov, and M. I. Yalandin, Generation of Subterahertz Superradiance Pulses based on Excitation of a Surface Wave by Relativistic Electron Bunches Moving in Oversized Corrugated Waveguides, Phys. Rev. Lett. **117**, 204801 (2016).
[22] J. Zhang, D. Zhang, Y. Fan, J. He, X. Ge, X. Zhang, J. Ju, and T. Xun, Progress in narrowband high-power microwave sources, Phys. Plasmas **27**, 010501 (2020).

[23] M. Friedman and V. Serlin, Modulation of Intense Relativistic Electron Beams by an External Microwave Source, Phys. Rev. Lett. **55**, 2860 (1985).
[24] J. Krall, M. Friedman, Y. Y. Lau, and V. Serlin, Simulation studies of a klystronlike amplifier operating in the 10–100 GW regime, IEEE Transactions on Electromagnetic Compatibility **34**, 222 (1992).
[25] J. Pasour, D. Smithe, and M. Friedman, The triaxial klystron, AIP Conf. Proc. **474**, 373 (1999).
[26] J. Ju, J. Zhang, Z. Qi, J. Yang, T. Shu, J. Zhang, and H. Zhong, Towards coherent combining of X-band high power microwaves: Phase-locked long pulse radiations by a relativistic triaxial klystron amplifier, Sci. Rep. **6**, 30657 (2016).
[27] J. Ju, J. Zhang, T. Shu, and H. Zhong, An improved X-band triaxial klystron amplifier for gigawatt long-pulse high-power microwave generation, IEEE Electron Device Lett. **38**, 270 (2017).
[28] See Supplemental Material at http://link.aps.org/supplemental/10.1103/PhysRevLett.130.085002 for more details regarding electromagnetic properties of the TKA cavities, pulsed magnetic field distribution, supporting experimental methods and results, PIC simulation, and phase analysis.
[29] G. Nusinovich, M. Read, and L. Song, Excitation of "monotron" oscillations in klystrons, Phys. Plasmas **11**, 4893 (2004).
[30] Y. Zhou, J. Ju, J. Zhang, W. Zhang, and F. Zhang, Design and optimization of reflectors in a relativistic triaxial klystron amplifier, IEEE Trans. Plasma Sci. **48**, 1923 (2020).
[31] J. Yang, Z. Zhang, H. Yang, J. Zhang, J. Liu, Y. Yin, T. Xun, X. Cheng, Y. Fan, Z. Jin, and J. Ju, Compact intense electron-beam accelerators based on high energy density liquid pulse forming lines, Matter Radiat. Extremes **3**, 278 (2018).
[32] J. Geng, J. Yang, X. Cheng, X. Yang, and R. Chen, The development of high-voltage repetitive low-jitter corona stabilized triggered switch, Rev. Sci. Instrum. **89**, 044705 (2018).
[33] CST Studio Suite at https://www.3ds.com/products-services/simulia/products/cst-studio-suite.
[34] J. Ju, W. Zhang, Y. Zhou, and J. Zhang, A large-size horn antenna for X-band high power microwave radiations, Rev. Sci. Instrum. **90**, 026101 (2019).
[35] W. Song, J. Sun, H. Shao, R. Xiao, C. Chen, and G. Liu, Inducing phase locking of multiple oscillators beyond the Adler's condition, J. Appl. Phys. **111**, 023302 (2012).
[36] G. A. Mesyats, N. S. Ginzburg, A. A. Golovanov, G. G. Denisov, I. V. Romanchenko, V. V. Rostov, K. A. Sharypov, V. G. Shpak, S. A. Shunailov, M. R. Ulmaskulov, M. I. Yalandin, and I. V. Zotova, Phase-Imposing Initiation of Cherenkov Superradiance Emission by an Ultrashort-Seed Microwave Pulse, Phys. Rev. Lett. **118**, 264801 (2017).
[37] M. Born and E. Wolf, *Principles of Optics*, 7th ed. (Cambridge University Press, Cambridge, 1999).
[38] J. Zhou, D. Liu, C. Liao, and Z. Li, CHIPIC: An efficient code for electromagnetic PIC modeling and simulation, IEEE Trans. Plasma Sci. **37**, 2002 (2009).
[39] Y. Y. Lau, Some design considerations on using modulated intense annular electron beams for particle acceleration, J. Appl. Phys. **62**, 351 (1987).
[40] R. M. Davis, R. L. Fante, and R. P. Perry, Phase-coded waveforms for radar, IEEE Trans. Aerosp. Electron. Syst. **43**, 401 (2007).
[41] G. Penco, E. Allaria, G. De Ninno, E. Ferrari, and L. Giannessi, Experimental Demonstration of Enhanced Self-Amplified Spontaneous Emission by an Optical Klystron, Phys. Rev. Lett. **114**, 013901 (2015).
[42] J. Amann *et al.*, Demonstration of self-seeding in a hard-x-ray free-electron laser, Nat. Photonics **6**, 393 (2012).